

Oxygen reduction for p-type TeO_x thin film transistor

Seiichi Kato¹, Masayuki Okamura¹, Tomomi Sawada¹, Toshihide Nabatame¹, and Kazuhito Tsukagoshi¹

¹ International Center for Materials Nanoarchitectonics (WPI-MANA), National Institute for Materials Science (NIMS), Tsukuba, Ibaraki 305-0044, Japan

Keywords: oxide transistor, p-type TFT, TeO_x, BEOL compatible, reducing agent, tungsten

Abstract

We investigated p-type TeO_x thin films fabricated by vacuum deposition using a mixture of TeO₂ powder and W powder in Al₂O₃ crucibles and evaluated its thin-film transistor (TFT) characteristics. P-Type TeO_x thin films were obtained when W was added at a weight ratio of 15% or more relative to TeO₂. However, the films became insulators and exhibited no electrical conductivity when the ratio was 10% or less. X-ray photoelectron spectroscopy analysis revealed that the TeO_x thin films contained approximately 5% or more Te–Te bonds. Because W–O bonds exhibit a higher dissociation energy than Te–O bonds, TeO₂ was considered to be reduced by W. In addition, W was not present in the film and was used solely for the reduction of TeO₂. When a W boat was used as the container for heating the evaporation source, quantitative analysis of the effects of the reduction by W was difficult. Therefore, an Al₂O₃ crucible, which reacts poorly with TeO₂, was used. The results showed that when TeO_x TFTs are fabricated by vacuum deposition, the addition of an appropriate amount of reducing agent to the raw material is essential to form an adequate amount of Te–Te bonds.

The advancement of information technology (IT) society demands higher performance and lower power consumption in semiconductors. To this end, the development of three-dimensional (3-D) integration of logic and memory is widely considered necessary.¹ Realizing this 3-D integration necessitates the monolithic 3-D integration of back-end-of-line (BEOL)-compatible logic and memory technologies based on complementary metal-oxide semiconductors (CMOSs).^{2,3} In BEOL technology, processes must be performed below 400°C to avoid damaging the BEOL metal interconnect layers; however, carrying out processes at such temperatures is difficult with Si.³ Amidst this, oxide semiconductors are gaining attention as alternatives to Si. In addition, demand exists for introducing CMOS technology into display circuits to achieve higher performance.⁴ Although CMOS devices require both n-type and p-type oxide transistors, the lack of high-performance p-type oxide transistors has prevented their practical implementation. Therefore, the realization of high-performance p-type oxide transistors is strongly demanded.

High-performance n-type oxide transistors have been realized. InGaZnO was first discovered by Kimizuka et al.⁵ and has been extensively researched^{6–8} and commercialized as an n-type material. InO_x,⁹ InCO,¹⁰ InSiO, InWO, and InTiO¹¹ have been widely studied and have achieved relatively stable electrical characteristics. However, no p-type semiconductors suitable for practical application have yet been reported. Cu₂O, NiO, and SnO are known p-type semiconductors;^{12,13} however, they are difficult to prepare as stable thin-film semiconductors because of problems such as property degradation. Among these materials, SnO is the most viable option, with numerous research results available.^{14–18} However, distinguishing between n-type SnO₂ and p-type SnO is difficult. Sputtering and evaporation methods often result in mixed phases, leading to poor transistor characteristics (e.g., low mobility and low on/off current ratios) when used as thin-film semiconductors. Achieving the practical application of SnO thin-film semiconductors is extremely challenging because of the difficulty in controlling these properties.¹⁹ Consequently, attention is increasingly shifting to p-type Te-based thin films.

Metal Te thin films are known to exhibit thin-film transistor (TFT) characteristics when used as p-type semiconductors.^{20–25} Examples of TFTs that simultaneously achieve high mobility and a high on/off ratio have been reported; however, they require special fabrication conditions such as cooling the substrate to –80°C during deposition to achieve high mobility.²⁶ TeO₂ has been predicted to exhibit stable characteristics as a p-type semiconductor,²⁷ and it has been the subject of extensive research.^{28–33} Recently, TFTs with high mobility and high on/off ratios were fabricated by doping TeO₂ with Se, attracting significant attention.³⁴ The addition of Se to the thin film has been speculated to result in p-type doping. However, no fundamental investigation into the conductivity of tellurium oxide has been reported, and no procedure or method for reliably producing semiconductor Te films has been

established. Te films are often prepared by vacuum deposition using TeO_2 powder placed on a W boat as the evaporation source. After the deposition, the W boat tends to undergo chemical reactions and discoloration. Determining how much W reacts during this process is not straightforward; quantitative analysis is difficult, and reproducibility is uncertain. In the present study, we used an Al_2O_3 crucible, which reacts poorly with TeO_2 and W, and fabricated thin films using a mixture of TeO_2 powder and W powder as the evaporation source. Our investigation of the effect of W revealed that the Te–Te bonds within the film play a crucial role in the manifestation of TFT characteristics.

A Si wafer (low-doped n-type Si) with a 200 nm thermal oxide layer was cut into 15 mm squares, cleaned with isopropyl alcohol and acetone, and then cleaned using an ultraviolet (UV) ozone cleaner. A conventional thermal evaporator was used to deposit thin films onto the substrates. The evaporation source was an Al_2O_3 crucible filled with a mixed powder of TeO_2 (Sigma-Aldrich, 99%) and W (Sigma-Aldrich, 99.9%). The average particle sizes of TeO_2 and W were 20 μm and 10 μm , respectively. The weight ratio of W to TeO_2 ranged from 0% to 55%. The thin film grew at a rate of 0.1 nm/s, with a thickness of approximately 20 nm. The vacuum level at evaporation was 8×10^{-4} Pa or lower, and the substrate was not cooled. The films were heat-treated at 225°C for 30 min in air after the evaporation. Ni electrodes (100 nm-thick) were subsequently attached by deposition onto the TeO_x channels. The TFT characteristics were measured under vacuum using a vacuum probe station (ZEST-8000-3-VSAPI, Nagase Electronic Equipment Service). XPS measurements (Quantera SXM, Ulvac Phi) and X-ray diffraction (XRD) measurements (SmartLab, Rigaku) were performed on TeO_x films. Secondary-ion mass spectrometry (SIMS, PHI ADEPT-1010, Ulvac Phi) measurements were also performed on a sample with 15% W to analyze its composition. In addition, the composition of the powdered raw material remaining in the crucible after vapor deposition was analyzed by XRD (Miniflex 600, Rigaku).

Figure 1 shows (a) photographs of a TeO_x TFT and (b) an overall view of the TeO_x TFT. The electrode spacing ranges from 50 to 350 μm , which does not affect electrical transport properties. The film with 15% W was thinned using the focused ion beam (FIB) method and subsequently observed using cross-sectional transmission electron microscopy (TEM) and nano-beam electron diffraction (JEM-ARM200F, JEOL) [Figs. 1(c) and (d)]. The inset shows the nano-beam electron diffraction pattern of the crystalline region. The majority of the film is amorphous, but some areas are crystallized. The electron diffraction patterns reveal that these crystallized regions are metallic Te crystals, not TeO_2 crystals. Measurements of the electrical properties reveal that the TFTs with a W ratio less than 10% exhibited insulating behavior, whereas those with a W ratio of 15% or greater displayed transistor characteristics. As an example, Fig. 1 shows the (e) output and (f) transfer curves for samples with 25% W and the (g) output and (h) transfer curves of the samples with 0% W. The TFT with 0% W is

an insulator, whereas that with 25% W exhibits p-type transistor characteristics. The field-effect hole mobility and on/off current ratio were extracted from the transfer curves. Their relationships with the weight ratio of W are plotted in Figs. 2(a) and 2(b). When the W ratio is 10% or less, the TeO_x film acts as an insulator and no current flows. However, when the W ratio is 15% or greater, the device exhibits TFT characteristics. As a general trend, with increasing W ratio, the mobility increases and the on/off ratio decreases.

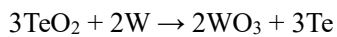
Figure 3(a) shows high-resolution XPS spectra of the Te 3d core-level for the film with 25% W. The main peaks are observed at the locations indicated by the red arrows (binding energy = 587, 576 eV), and the satellite peaks are observed at the locations indicated by the blue arrows (binding energy = 583, 573 eV). These peaks originate from the $3d_{3/2}$ and $3d_{5/2}$ orbitals of Te, respectively. The two main peaks originate from Te–O bonds, whereas the two satellite peaks originate from Te–Te bonds. Therefore, the ratio of Te–O bonds to Te–Te bonds can be estimated from the intensity ratio between the main peak and the satellite peak. The inset shows the XPS results for the 0% W sample before it was annealed. Satellite peaks are scarcely observed, indicating that the sample contains few Te–Te bonds. The intensity of each peak was estimated from its area, and the ratio of Te–Te bonds across the entire observed region was calculated. Background processing was performed using the Tougaard method.³⁵ The results for the as-grown film were omitted because its satellite peaks were extremely broad, making analysis difficult. Figure 3(b) shows the relationship between the W weight ratio and the ratio of Te–Te bonds. The white and black square values were calculated from the $3d_{5/2}$ and $3d_{3/2}$ peaks, respectively. The peak intensity ratios of the $3d_{5/2}$ and $3d_{3/2}$ peaks are nearly consistent. A trend is observed where the Te–Te ratio tends to increase with increasing W concentration, indicating that the greater the concentration of W, the greater the proportion of Te–Te bonds. For films with a W ratio of 15% or greater, the Te–Te bond content is approximately 5% or higher; however, for films with a W ratio less than 10%, the Te–Te bond content is less than 5%. Because conductivity is exhibited when the W ratio is 15% or higher, a Te–Te bond content of 5% or more is required to attain TFT characteristics. No peaks attributable to W were observed in the wide-scan (low-resolution) XPS spectra of any of the films. In addition, the presence of W atoms could not be confirmed from the SIMS measurement results, indicating that the film does not contain W atoms.

Thin-film X-ray measurements were performed to examine the sample structures. Figure 4(a) shows the diffraction patterns for films with W ratios of 15%, 35%, and 55%. The Miller indices are for the metallic Te crystal. The three films exhibit current modulation in their gate-voltage change. Overall, the films are amorphous; however, weak peaks corresponding to metallic Te crystals are observed. Compared with the peaks of the sample with 15% W, those of the samples with greater W ratios (e.g., 35% and 55%) are slightly more intense. Therefore, the films with W ratios of 35% and 55% are

considered to contain more Te crystals than the film with a W ratio of 15%. No clear difference is observed between the diffraction pattern for the film with 35% W and that of the film with 55% W. The XPS results indicate that the amount of Te crystals increases with increasing W ratio in the raw material. The XRD results show differences between the film with 15% W and that with 55% W but not between the film with 35% W and that with 55% W. Figure 3(b) shows that the difference in the Te–Te ratios between the films with 35% and 55% W is small compared with the difference between the films with 15% and 35% W. Therefore, the lack of distinct differences in the XRD patterns is reasonable.

Even when thin films were formed using pure TeO₂ as the evaporation source, neither conductivity nor semiconductor characteristics were observed. Introducing W into TeO₂ generated an appropriate proportion of Te–Te bonds, leading to conductivity and semiconductor characteristics. To adjust the proportion of Te–Te bonds, we mixed W powder into the TeO₂ powder. The W powder reduced the TeO₂, decreased the abundance of Te–O bonds, and increased the abundance of Te–Te bonds. The dissociation energy of the Te–O bond (377 kJ/mol) is lower than that of the W–O bond (720 kJ/mol). Therefore, the W–O bond is more stable. The oxygen in the Te–O bond is pulled toward the W, leading to the phenomenon described above.

The powdered raw material remaining in the crucible after vapor deposition of the films with 45% W was analyzed by XRD [Fig. 4(b)]. The black, blue, and red triangles in Fig. 4(b) indicate peaks originating from TeO₂, W, and WO₃, respectively. The results show that WO₃, which did not exist prior to vapor deposition, is present. Potential sources of oxygen for W include TeO₂ and/or the crucible's Al₂O₃. The dissociation energy for the Al–O bond is 502 kJ/mol, which is greater than that for Te–O but less than that for W–O. Therefore, TeO₂ can supply oxygen to W more easily than Al₂O₃. In addition, the W powder is thoroughly mixed with the TeO₂ powder and only slightly contacts the Al₂O₃ crucible at the crucible surface. Therefore, the primary source of oxygen supplied to the W is the TeO₂ powder. The following reaction is considered to have occurred within the crucible:



The dependence of the XPS and XRD peak intensities on the W ratio indicates that increasing the W ratio in the raw material increases the amount of Te–Te bonds and also increases the amount of metallic Te crystals. Consequently, an increase in the conductive metal component within the TeO_x film leads to higher mobility, and an increase in the off-current causes a decrease in the on/off ratio. Therefore, to obtain a high-performance TFT, the appropriate amount of W must be added. W is used solely for the reduction of the raw material (TeO₂) and does not enter the sample itself to cause any effect. The

melting point of W ($>3380^{\circ}\text{C}$) is substantially higher than that of TeO_2 (733°C); the W is therefore unlikely to evaporate at the temperatures used for depositing TeO_2 at a low rate of 0.1 nm/s . In addition, films were prepared using powders of Si (799 kJ/mol) or C (1076 kJ/mol), which have Si–O and C–O bond dissociation energies greater than that of Te–O, and their TFT characteristics were investigated using the same method. TFT characteristics were achieved both for the sample mixed with 25% Si by weight relative to TeO_2 and for the sample mixed with 25% C by weight relative to TeO_2 .

The XRD and electron diffraction results indicate that samples exhibiting TFT characteristics contain trace amounts of metallic Te crystals. In addition, the XPS measurements reveal that thin films exhibiting TFT characteristics contain a certain amount of Te–Te bonds. These results suggest that the presence of a moderate amount of Te–Te bonds is essential for achieving TFT characteristics. The conventional method using W boats made quantitatively analyzing the influence of W difficult; however, the method used in the present study enables accurate measurement of the amount of W in the raw material. This approach both enables quantitative analysis and improves the reproducibility. In addition, because there are no heating steps other than the 225°C heat treatment after vapor deposition throughout the entire process, the proposed method is compliant with the requirement of temperatures of 400°C or lower for BEOL-compatible systems.

In this work, we fabricated amorphous TeO_2 thin films using vacuum evaporation with a low-reactivity Al_2O_3 crucible. We mixed W powder into the TeO_2 powder raw material and investigated the relationship between the W ratio and electrical properties of the resultant films. When W was mixed at a weight ratio of 15% or more relative to TeO_2 , films with electric conduction with p-type TFT characteristics were obtained. However, when the W ratio was 10% or less, the material became an insulator and did not exhibit TFT characteristics. The results of XPS analyses, thin-film XRD measurements, and TEM observations revealed that films exhibiting TFT characteristics form fine Te crystals and exhibit an increase in Te–Te bonds. A Te–Te bond content of at least 5% within the sample is considered essential to attain TFT characteristics. In addition, because the entire process is conducted below 400°C , it can be used with BEOL-compatible systems.

The authors are grateful to Prof. D. H. Lien, Dr. T. Onaya, and Dr. H. Yoshikawa for useful discussions. This research was conducted with the support of NIMS Open Facility Surface and Bulk Analysis Unit (SBU).

AUTHOR DECLARATIONS

Conflict of Interest

The authors have no conflicts to disclose.

Author Contributions

Seiichi Kato: Data curation (lead); Investigation (lead); Writing – original draft (lead); Writing – review & editing (lead). Masayuki Okamura: Data curation (supporting). Tomomi Sawada: Data curation (supporting). Toshihide Nabatame: Data curation (supporting); Investigation (supporting). Kazuhito Tsukagoshi: Data curation (supporting); Investigation (equal); Writing – original draft (supporting); Writing – review & editing (equal).

DATA AVAILABILITY

The data that support the findings of this study are available within the article.

REFERENCES

- ¹ M.M. Sabry Aly, T.F. Wu, A. Bartolo, Y.H. Malviya, W. Hwang, G. Hills, I. Markov, M. Wootters, M.M. Shulaker, H.-S. Philip Wong, and S. Mitra, “The N3XT approach to energy-efficient abundant-data computing,” *Proc. IEEE* **107**(1), 19–48 (2019).
- ² T. Srimani, A. Bechdolt, S. Choi, C. Gilardi, A. Kasperovich, S. Li, Q. Lin, M. Malakoutian, P. McEwen, R.M. Radway, D. Rich, A.C. Yu, S. Fuller, S. Achour, S. Chowdhury, H.-S.P. Wong, M. Shulaker, and S. Mitra, “N3XT 3D technology foundations and their lab-to-fab: omni 3D logic, logic+memory ultra-dense 3D, 3D thermal scaffolding,” in *2023 International Electron Devices Meeting (IEDM)*, (2023), pp. 1–4.
- ³ W. Wang, K. Li, J. Lan, M. Shen, Z. Wang, X. Feng, H. Yu, K. Chen, J. Li, F. Zhou, L. Lin, P. Zhang, and Y. Li, “CMOS backend-of-line compatible memory array and logic circuitries enabled by high performance atomic layer deposited ZnO thin-film transistor,” *Nat Commun* **14**(1), 6079 (2023).
- ⁴ S.C. Jang, J. Shim, H. Jang, Y. Lee, S. Biswas, J. Park, H. Shin, H. Kim, S. Kim, and H.-S. Kim, “Recent progress in the development of backplane thin-film transistors for information displays,” *Journal of Information Display* **26**(4), 341–356 (2025).
- ⁵ N. Kimizuka and T. Mohri, “Spinel, YbFe₂O₄, and Yb₂Fe₃O₇ types of Structures for compounds in the In₂O₃ and Sc₂O₃-A₂O₃-BO systems [A: Fe, Ga, or Al; B: Mg, Mn, Fe, Ni, Cu, or Zn] at temperatures over 1000°C”, *J. Solid State Chem.* **60** 382-384 (1985).
- ⁶ K. Nomura, H. Ohta, A. Takagi, T. Kamiya, M. Hirano, and H. Hosono, “Room-temperature fabrication of transparent flexible thin-film transistors using amorphous oxide semiconductors,”

Nature **432**(7016), 488–492 (2004).

⁷ H. Kunitake, R. Arasawa, T. Seki, R. Honda, H. Baba, D. Shimada, H. Kimura, R. Tokumaru, T. Atsumi, K. Kato, S. Yamazaki, K. Ohshima, K. Tsuda, N. Matsumoto, T. Koshida, S. Ohshita, H. Sawai, Y. Yanagisawa, and S. Saga, “A c-axis-aligned crystalline In-Ga-Zn oxide FET with a gate length of 21 nm suitable for memory applications,” IEEE J. Electron Devices Soc. **7**, 495–502 (2019).

⁸ N. Yoshida, J.P. Bermundo, Y. Ishikawa, T. Nonaka, K. Taniguchi, and Y. Uraoka, “Low temperature cured poly-siloxane passivation for highly reliable *a* -InGaZnO thin-film transistors,” Applied Physics Letters **112**(21), 213503 (2018).

⁹ M. Si, Z. Lin, Z. Chen, X. Sun, H. Wang, and P.D. Ye, “Scaled indium oxide transistors fabricated using atomic layer deposition,” Nat Electron **5**(3), 164–170 (2022).

¹⁰ R. Kobayashi, T. Nabatame, T. Onaya, A. Ohi, N. Ikeda, T. Nagata, K. Tsukagoshi, and A. Ogura, “Comparison of characteristics of thin-film transistor with In₂O₃ and carbon-doped In₂O₃ channels by atomic layer deposition and post-metallization annealing in O₃,” Jpn. J. Appl. Phys. **60**(3), 030903 (2021).

¹¹ S. Aikawa, T. Nabatame, and K. Tsukagoshi, “Effects of dopants in InO_x-based amorphous oxide semiconductors for thin-film transistor applications,” Appl. Phys. Lett. **103**(17), 172105 (2013).

¹² Z.-W. Shang, H.-H. Hsu, Z.-W. Zheng, and C.-H. Cheng, “Progress and challenges in p-type oxide-based thin film transistors,” Nanotechnology Reviews **8**(1), 422–443 (2019).

¹³ G. Byeon, S.C. Jang, T. Roh, J.-M. Park, H.-S. Kim, and Y.-Y. Noh, “Recent progress in the development of backplane thin film transistors for information displays,” Journal of Information Display **24**(3), 159–168 (2023).

¹⁴ I-Chung Chiu, Yun-Shiuan Li, Min-Sheng Tu, and I-Chun Cheng, “Complementary oxide–semiconductor-based circuits with n-channel ZnO and p-channel SnO thin-film transistors,” IEEE Electron Device Lett. **35**(12), 1263–1265 (2014).

¹⁵ Y.-S. Li, J.-C. He, S.-M. Hsu, C.-C. Lee, D.-Y. Su, F.-Y. Tsai, and I.-C. Cheng, “Flexible complementary oxide–semiconductor-based circuits employing n-channel ZnO and p-channel SnO thin-film transistors,” IEEE Electron Device Lett. **37**(1), 46–49 (2016).

¹⁶ H. Yabuta, N. Kaji, R. Hayashi, H. Kumomi, K. Nomura, T. Kamiya, M. Hirano, and H. Hosono, “Sputtering formation of p-type SnO thin-film transistors on glass toward oxide complimentary circuits,” (2026).

¹⁷ J. Yang, Y. Wang, Y. Li, Y. Yuan, Z. Hu, P. Ma, L. Zhou, Q. Wang, A. Song, and Q. Xin, “Highly optimized complementary inverters based on p-SnO and n-InGaZnO with high uniformity,” IEEE Electron Device Lett. **39**(4), 516–519 (2018).

¹⁸ Y. Ogo, H. Hiramatsu, K. Nomura, H. Yanagi, T. Kamiya, M. Hirano, and H. Hosono, “p-channel thin-film transistor using p-type oxide semiconductor, SnO,” Applied Physics Letters **93**(3), 032113 (2008).

- ¹⁹ Y.-L. Sun, T. Nabatame, J.W. Chung, T. Sawada, H. Miura, M. Miyamoto, and K. Tsukagoshi, “Compositional changes between metastable SnO and stable SnO₂ in a sputtered film for p-type thin-film transistors,” *Thin Solid Films* **807**, 140548 (2024).
- ²⁰ Y. Wang, G. Qiu, R. Wang, S. Huang, Q. Wang, Y. Liu, Y. Du, W.A. Goddard, M.J. Kim, X. Xu, P.D. Ye, and W. Wu, “Field-effect transistors made from solution-grown two-dimensional tellurene,” *Nat Electron* **1**(4), 228–236 (2018).
- ²¹ G. Zhou, R. Addou, Q. Wang, S. Honari, C.R. Cormier, L. Cheng, R. Yue, C.M. Smyth, A. Laturia, J. Kim, W.G. Vandenberghe, M.J. Kim, R.M. Wallace, and C.L. Hinkle, “High-mobility helical tellurium field-effect transistors enabled by transfer-free, low-temperature direct growth,” *Advanced Materials* **30**(36), 1803109 (2018).
- ²² T. Kim, C.H. Choi, S.E. Kim, J.-K. Kim, J. Jang, S. Choi, J. Noh, K.-S. Park, J. Kim, S. Yoon, and J.K. Jeong, “High-performance hexagonal tellurium thin-film transistor using tellurium oxide as a crystallization retarder,” *IEEE Electron Device Lett.* **44**(2), 269–272 (2023).
- ²³ M. Kim, Y. Lee, K. Kim, G.-H. Pham, K. Kim, J.H. Jun, H. Lee, S. Yoon, H.J. Hwang, M.M. Sung, and B.H. Lee, “Processes to enable hysteresis-free operation of ultrathin ALD Te p-channel field-effect transistors,” *Nanoscale Horiz.* **9**(11), 1990–1998 (2024).
- ²⁴ H. Zhu, L. Fan, K. Wang, H. Liu, J. Zhang, and S. Yan, “Progress in the synthesis and application of tellurium nanomaterials,” *Nanomaterials* **13**(14), 2057 (2023).
- ²⁵ T. Kawaguchi, Y. Tanaka, H. Sekiguchi, H. Hirai, K. Sato, and S. Kobayashi, “A novel method of fabricating Te thin-film transistors,” *Jpn. J. Appl. Phys.* **25**(3R), 449 (1986).
- ²⁶ C. Zhao, C. Tan, D.-H. Lien, X. Song, M. Amani, M. Hettick, H.Y.Y. Nyein, Z. Yuan, L. Li, M.C. Scott, and A. Javey, “Evaporated tellurium thin films for p-type field-effect transistors and circuits,” *Nat. Nanotechnol.* **15**(1), 53–58 (2020).
- ²⁷ J. Robertson, X. Zhang, Q. Gui, and Y. Guo, “Amorphous TeO₂ as p-type oxide semiconductor for device applications,” *Applied Physics Letters* **124**(21), 212101 (2024).
- ²⁸ N. Devabharathi, S. Yadav, I. Dönges, V. Trouillet, and J.J. Schneider, “ α -TeO₂ oxide as transparent p-type semiconductor for low temperature processed thin film transistor devices,” *Adv Materials Inter* **11**(16), 2301082 (2024).
- ²⁹ S. Moufok, L. Kadi, B. Amrani, and K.D. Khodja, “Electronic structure and optical properties of TeO₂ polymorphs,” *Results in Physics* **13**, 102315 (2019).
- ³⁰ J. Robertson, X. Zhang, Q. Gui, and Y. Guo, “Amorphous TeO₂ as p-type oxide semiconductor for BEOL applications,” in *2024 International VLSI Symposium on Technology, Systems and Applications (VLSI TSA)*, (IEEE, HsinChu, Taiwan, 2024), pp. 1–2.
- ³¹ S. Guo, Z. Zhu, X. Hu, W. Zhou, X. Song, S. Zhang, K. Zhang, and H. Zeng, “Ultrathin tellurium dioxide: emerging direct bandgap semiconductor with high-mobility transport anisotropy,” *Nanoscale* **10**(18), 8397–8403 (2018).

- ³² C. Niu, P. Tan, J.-Y. Lin, L. Long, Z. Lin, Y. Zhang, H. Wang, G.D. Wilk, and P.D. Ye, “First demonstration of BEOL wafer-scale all-ALD channel CFETs using IGZO and Te for monolithic 3D integration,” in *2024 IEEE International Electron Devices Meeting (IEDM)*, (IEEE, San Francisco, CA, USA, 2024), pp. 1–4.
- ³³ P. Tan, C. Niu, Z. Lin, J.-Y. Lin, L. Long, Y. Zhang, G. Wilk, H. Wang, and P.D. Ye, “Wafer-scale atomic layer-deposited TeO_x/Te heterostructure p-type thin-film transistors,” *Nano Lett.* **24**(40), 12433–12441 (2024).
- ³⁴ A. Liu, Y.-S. Kim, M.G. Kim, Y. Reo, T. Zou, T. Choi, S. Bai, H. Zhu, and Y.-Y. Noh, “Selenium-alloyed tellurium oxide for amorphous p-channel transistors,” *Nature* **629**(8013), 798–802 (2024).
- ³⁵ S. Tougaard, “Quantitative analysis of the inelastic background in surface electron spectroscopy,” *Surface & Interface Analysis* **11**(9), 453–472 (1988).

Figure Captions

Figure 1

(a) Photograph of a TeO_x TFT. (b) Overall view of the TeO_x TFT fabricated on a 15 mm square Si substrate. The electrode spacing ranges from 50 to 350 nm. (c) Cross-sectional TEM image and (d) a corresponding enlarged view of the sample with 15% W. The inset shows the nano-beam electron diffraction pattern of the crystalline region. The majority of the film is amorphous, but some areas are crystallized. Analysis revealed that the film was a metallic Te crystal. (e) Output and (f) transfer curves for samples with 25% W and (g) output and (h) transfer curves for samples with 0% W. The sample with 0% W is an insulator, whereas the sample with 25% W exhibits p-type transistor characteristics.

Figure 2

Correlation between the W-to-TeO₂ weight ratio and (a) the field-effect hole mobility and (b) the on/off current ratio. When the W ratio is 10% or less, the film acts as an insulator and no current flows. However, when the W ratio is 15% or greater, the film exhibits TFT characteristics. When the W ratio is 15% or greater, as a general trend, the mobility increases and the on/off ratio decreases with increasing W ratio.

Figure 3

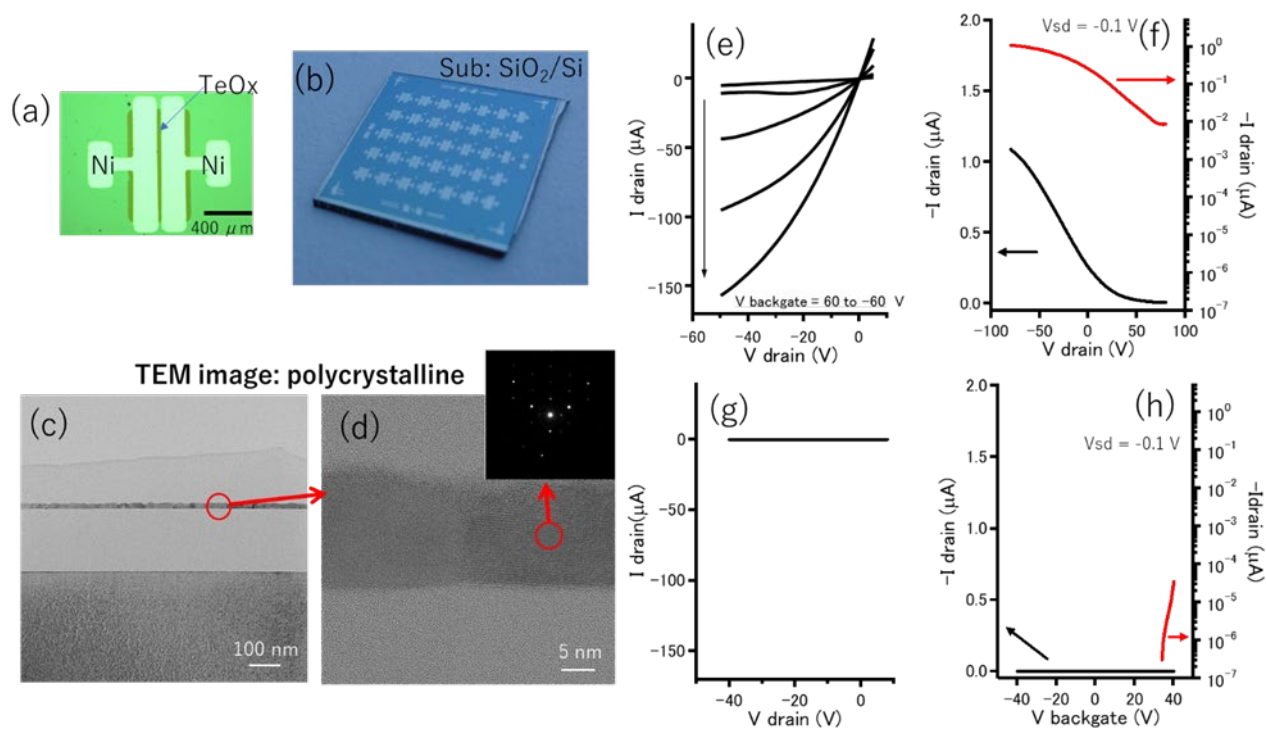
(a) High-resolution Te 3d core-level spectra for the sample with 25% W. The main peaks are observed at the locations indicated by the red arrows (binding energy = 587, 576 eV), and the satellite peaks are observed at the locations indicated by the blue arrows (binding energy = 583, 573 eV). These peaks originate from the 3d_{3/2} and 3d_{5/2} orbitals of Te, respectively. The two main peaks originate from Te–

O bonds, whereas the two satellite peaks originate from Te–Te bonds. The inset shows the XPS results for the sample with 0% W prior to annealing. Satellite peaks are scarcely observed, indicating that almost no Te–Te bonds are present. (b) The relationship between the weight ratio of W and the ratio of Te–Te bonds. The white and black square values were calculated from the 3d_{5/2} and 3d_{3/2} peaks, respectively. A trend is observed where the intensity ratio tends to increase with increasing W ratio. That is, the greater the amount of W, the greater the proportion of Te–Te bonds.

Figure 4

(a) X-ray diffraction pattern of samples in which the W-to-TeO₂ weight ratio is 15%, 35%, and 55%. The Miller indices are for the metallic Te crystal. All of the films exhibit TFT characteristics. (b) X-ray diffraction pattern of the raw material powder remaining in the crucible after evaporation of the film with 45% W. The black, blue, and red triangles indicate peaks originating from TeO₂, W, and WO₃, respectively. WO₃, which did not exist prior to vapor deposition, is present. W was oxidized by consuming O₂ from its surroundings.

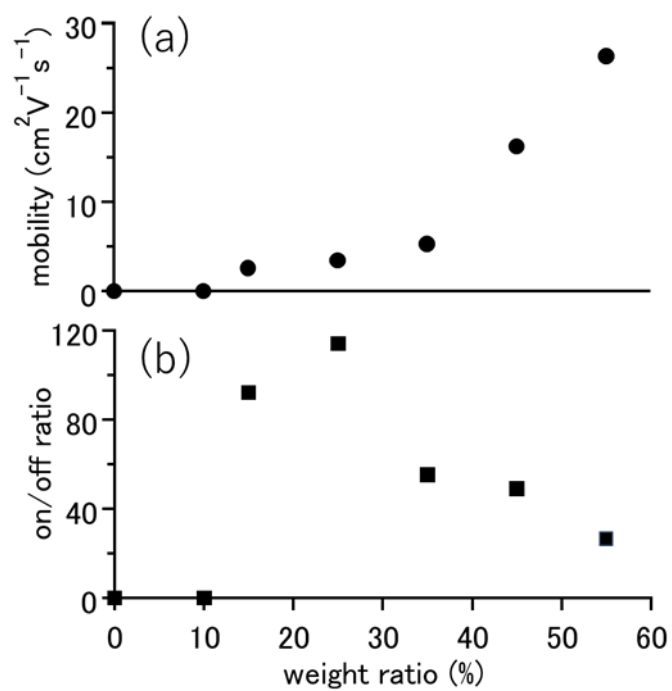
397 Figure 1



398

399

400 Figure 2



401

402

403

Figure 3

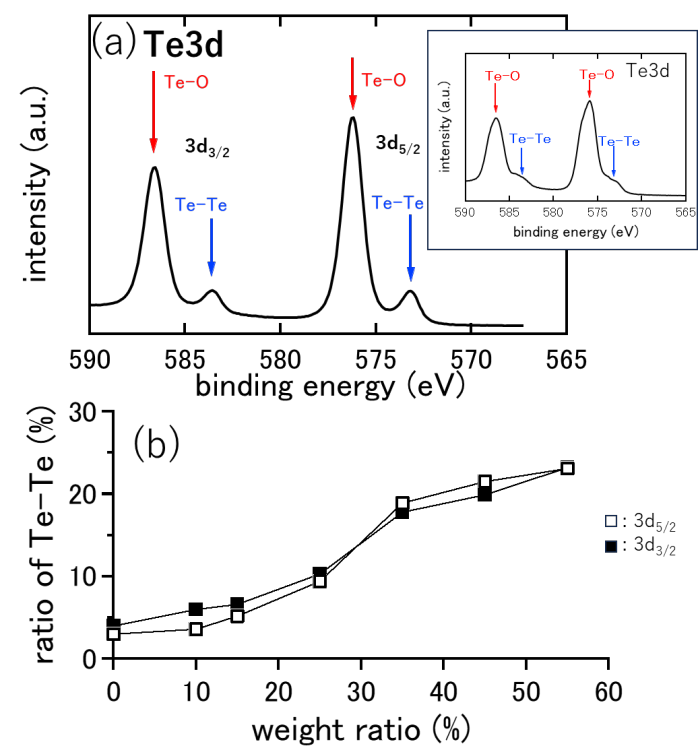


Figure 4

